

# The radio-loud narrow-line Seyfert 1 galaxy 1H 0323+342 in a galaxy merger

Akihiro Doi,<sup>1,2★</sup> Motoki Kino<sup>3,4</sup>, Nozomu Kawakatu<sup>5</sup> and Kazuhiro Hada<sup>6,7</sup>

<sup>1</sup>*The Institute of Space and Astronautical Science, Japan Aerospace Exploration Agency, 3-1-1 Yoshinodai, Chuou-ku, Sagami-hara, Kanagawa 252-0292, Japan*

<sup>2</sup>*Department of Space and Astronautical Science, SOKENDAI, 3-1-1 Yoshinodai, Chuou-ku, Sagami-hara, Kanagawa 252-5210, Japan*

<sup>3</sup>*Kogakuin University of Technology & Engineering, Academic Support Center, 2665-1 Nakano, Hachioji, Tokyo 192-0015, Japan*

<sup>4</sup>*National Astronomical Observatory of Japan, 2-21-1 Osawa, Mitaka, Tokyo 181-8588, Japan*

<sup>5</sup>*National Institute of Technology, Kure College, 2-2-11, Agaminami, Kure, Hiroshima 737-8506, Japan*

<sup>6</sup>*Mizusawa VLBI Observatory, National Astronomical Observatory of Japan, 2-12 Hoshigaoka, Mizusawa, Oshu, Iwate 023-0861, Japan*

<sup>7</sup>*Department of Astronomical Science, SOKENDAI, 2-21-1 Osawa, Mitaka, Tokyo 181-8588, Japan*

Accepted 2020 May 20. Received 2020 May 19; in original form 2019 June 17

## ABSTRACT

The supermassive black holes (SMBHs) of narrow-line Seyfert 1 galaxies (NLS1s) are at the lowest end of mass function of active galactic nuclei (AGNs) and preferentially reside in late-type host galaxies with pseudobulges, which are thought to be formed by internal secular evolution. On the other hand, the population of radio-loud NLS1s presents a challenge for the relativistic jet paradigm that powerful radio jets are exclusively associated with very high mass SMBHs in elliptical hosts, which are built-up through galaxy mergers. We investigated distorted radio structures associated with the nearest gamma-ray emitting, radio-loud NLS1 1H 0323+342. This provides supporting evidence for the merger hypothesis based on the past optical/near-infrared observations of its host galaxy. The anomalous radio morphology consists of two different structures, the inner curved structure of currently active jet and the outer linear structure of low-brightness relics. Such a coexistence might be indicative of the stage of an established black hole binary with precession before the black holes coalesce in the galaxy merger process. 1H 0323+342 and other radio-loud NLS1s under galaxy interactions may be extreme objects on the evolutionary path from radio-quiet NLS1s to normal Seyfert galaxies with larger SMBHs in classical bulges through mergers and merger-induced jet phases.

**Key words:** galaxies: active — galaxies: Seyfert — galaxies: jets — radio continuum: galaxies — galaxies: individual (1H 0323+342) — gamma rays: galaxies

## 1 INTRODUCTION

The scaling relation between the masses of supermassive black holes (SMBHs) and spheroidal components in galaxies suggests the regulated co-evolution of SMBHs and galaxies (e.g., Magorrian et al. 1998; Gebhardt et al. 2000; Ferrarese & Merritt 2000). Elliptical galaxies with very high-mass SMBHs are thought to be the end products through major mergers with the active galactic nucleus (AGN) feedback mechanism in the quasar era (e.g., Hopkins et al. 2008; Kormendy & Ho 2013). The relation has been established from the samples of elliptical galaxies and disk galaxies with classical bulges hosting SMBHs with relatively large masses ( $\gtrsim 10^7 M_\odot$ ). On the other hand,

narrow-line Seyfert 1 (NLS1) galaxies are a class of AGNs at the lowest end of the SMBH mass function in the local universe ( $\lesssim 10^7 M_\odot$ ; e.g., Peterson 2011; Woo et al. 2015). The samples of active and inactive galaxies with low-mass SMBHs leads to a significant deviation from the linear relation between the black hole and spheroid stellar masses (e.g., Kormendy & Ho 2013; Graham & Scott 2015; Davis et al. 2019). This is suggestive of a different evolutionary track in the low-mass regime. NLS1 engines predominantly reside in late-type galaxies (Deo et al. 2006) with pseudo-bulges (Orban de Xivry et al. 2011; Mathur et al. 2011). Optical observations of host morphology suggests the paucity of the signature of galaxy interactions (Ryan et al. 2007; Ohta et al. 2007), in addition to the prevalence of strongly barred spirals/disks (Crenshaw et al. 2003; Deo et al. 2006; Ohta et al. 2007). These characteristics are indications of

★ E-mail: doi.akihiro@jaxa.jp

the internal secular evolution, rather than major mergers, for the growing processes of NLS1s' central black holes and host galaxies (Kormendy & Kennicutt 2004).

Meanwhile, the radio jet activity potentially has a strong link with the co-evolution of SMBHs and galaxies. The relativistic-jet paradigm is known in which radio galaxies and blazars are associated exclusively with elliptical host galaxies harboring very high mass SMBHs (Kotilainen et al. 1998b,a; Laor 2000; Sikora et al. 2007), with only several exceptions (Ledlow et al. 1998; Keel et al. 2006; Hota et al. 2011; Bagchi et al. 2014; Mao et al. 2015; Singh et al. 2015). Additionally, a big fraction of the host galaxies of radio-loud AGNs are associated with recent or ongoing merger events (92% $^{+14\%}_{-8\%}$  at  $z > 1$ , Chiaberge et al. 2015; 93% at  $z < 0.2$  and 95% at  $0.2 \leq z < 0.7$ , Ramos Almeida et al. 2012), suggesting a strong link with the relativistic jet triggering mechanism. Most of the NLS1s ( $\sim 93\%$ ) are radio-quiet<sup>1</sup> ( $R < 10$ ; Zhou et al. 2006; Komossa et al. 2006), indicating poor jet activities as a class. Therefore, the hypothesis that the SMBHs of radio-quiet NLS1s are growing in the internal secular process without merger events could be understood as a population out of the framework of the relativistic jet paradigm + merger-triggered jet activity.

On the other hand, radio-loud objects do exist in the NLS1 population. Observational evidence that the jet activity of the radio-loud NLS1s is associated with host morphology and merger events is still under exploration. Since most of radio-loud NLS1s are distant objects, optical/near-infrared observations for investigating their host morphology are relatively difficult. There have been some reports for  $\gamma$ -ray emitting NLS1s: PKS 1502+036 possibly in an elliptical (D'Ammando et al. 2018), FBQS J1644+2619 possibly in an elliptical (D'Ammando et al. 2017) or a barred lenticular galaxy with a pseudobulge possibly in a minor merger (Olguín-Iglesias et al. 2017), PKS 2004-447 in the host with a pseudobulge (Kotilainen et al. 2016), and 1H 0323+342 in a host galaxy showing a spiral (Zhou et al. 2007) or ring-like morphology suggestive of a merger (Antón et al. 2008). For the radio-loud (not  $\gamma$ -ray-detected) NLS1s, spiral hosts with pseudobulge and galaxy-interaction/disturbance indications were found in J111934.01+533518.7 and J161259.83+421940.3 (Järvelä et al. 2018) and an observation suggests that IRAS 20181-2244 is hosted by a late-type galaxy in an interacting system of two galaxies (Berton et al. 2019). Recently, Olguín-Iglesias et al. (2020) reported the results of deep near-infrared imaging for 29 radio-loud NLS1s, strongly indicating that their hosts are preferentially disc galaxies with the signs of pseudobulges (16 sources) and galaxy interaction (18 sources). Six radio-loud NLS1s show an offset stellar bulge with respect to the AGN, suggesting distorted morphology due to a galaxy merger. These properties are suggestive of merger-induced jet activity, but are inconsistent with the relativistic-jet paradigm in which radio-loud AGNs are exclusively in elliptical hosts. If NLS1s are young objects eventually evolving into broad-line Seyfert galaxies with larger mass SMBHs (Mathur 2000), radio-loud NLS1s

could be extreme objects on the evolutionary path from radio-quiet NLS1s to broad-line Seyferts (Doi et al. 2012) through merger processes. The fueling mechanism driven by minor majors has been proposed for the nuclear activity of broad-line Seyfert galaxies (Taniguchi 1999).

Radio observations provide another approach to explore the history of host galaxy's merger by investigating distorted radio morphology that possibly contains traces of the history of jet activity. X-shaped radio galaxies usually consist of a pair of Fanaroff–Riley class II (FR II)-like radio arms with active lobes (“primary lobes”) and a pair of lower-brightness lobes with no hotspots (“secondary lobes” or “wings”) as relics. The physical origin of the X-shaped radio galaxies is often discussed in the framework of (1) the spin-flip scenario, (2) hydrodynamic effects, and (3) the precession model. The spin-flip scenario postulates a change of the jet direction due to a sudden flip of black hole's spin axis through a coalescence with another black hole in the final stage of a galactic merger (e.g., Merritt & Ekers 2002). The hydrodynamic effects as an interaction with the surrounding interstellar medium in a merger environment (the backflow diversion model (e.g., Leahy & Williams 1984; Capetti et al. 2002); the jet-shell interaction model (Gopal-Krishna et al. 2012)) are considered if a characteristically distorted structure is apparent in secondary lobes. The precessing jet in a binary black hole system formed via a merger (e.g., Begelman et al. 1980; Liu & Chen 2007) is postulated in the middle stage of a galactic merger before two black holes coalesce, if a helically curved jet structure is observed. For investigating the merger experience of radio-loud NLS1s, the large radio structure that tends to exceed the galaxy scale and the high spatial resolution of radio interferometry could surpass optical observation approaches.

1H 0323+342 is the nearest ( $z = 0.0629$ ; Zhou et al. 2007) object among known  $\gamma$ -ray-emitting NLS1s (Abdo et al. 2009; Paliya et al. 2014). Thanks to its proximity, 1H 0323+342 is one of the best sources that can be investigated by direct imaging of jet activity and host galaxy. The host galaxy has been resolved on some level and exhibits a one-armed spiral (Zhou et al. 2007) or ring-like morphology, likely associated with a recent violent dynamical interaction of the host galaxy (Antón et al. 2008; León Tavares et al. 2014; Olguín-Iglesias et al. 2020). The analyses of the bulge profile show a Sérsic index of  $n = 0.88/1.24$  at the J/K-band (Olguín-Iglesias et al. 2020; see also León Tavares et al. 2014 who reported  $n \sim 1.2$  based on their model B), suggesting a pseudobulge ( $n < 2$ ; Fisher & Drory 2008). The black hole mass is certainly low:  $3.4 \times 10^7 M_\odot$  based on reverberation mapping (Wang et al. 2016), which is consistent with estimations based on the X-ray variability ( $\lesssim 1\text{--}4 \times 10^7 M_\odot$ ; Yao et al. 2015; Landt et al. 2017; Pan et al. 2018) and the single-epoch relation between the line width and luminosity ( $\sim 1\text{--}3 \times 10^7 M_\odot$ ; Zhou et al. 2007; León Tavares et al. 2014), but is an order of magnitude smaller than that given by the black hole–bulge mass relation (León Tavares et al. 2014). The parsec (pc)-scale radio jet is highly relativistic showing a one-sided structure and superluminal motions (Wajima et al. 2014; Fuhrmann et al. 2016; Lister et al. 2016; Doi et al. 2018; Hada et al. 2018). For kpc-scale radio structure, Antón et al. (2008) presented two radio images showing a core plus a two-sided structure with unusual morphology.

<sup>1</sup> Radio-loudness  $R$  is defined as the ratio of the 5 GHz to the optical B-band fluxes (Kellermann et al. 1989). A source is considered radio-loud if  $R > 10$ .

Antón et al. (2008) briefly discussed the possibility of merger-induced morphology for the anomalous radio jet structure of 1H 0323+342. No more detailed studies have been made so far for the kpc-scale radio structure of 1H 0323+342.

In the present paper, for 1H 0323+342 we report a detailed investigation of radio morphology, indicating the history of changing jet axis. We assume a  $\Lambda$ CDM cosmology with  $H_0 = 70.5 \text{ km s}^{-1} \text{ Mpc}^{-1}$ ,  $\Omega_M = 0.27$ , and  $\Omega_\Lambda = 0.73$ . At the distance to 1H 0323+342, an angular size of  $1''$  corresponds to 1.2 kpc in the projected distance.

## 2 DATA AND RADIO IMAGES

We retrieved the Karl G. Jansky Very Large Array (VLA<sup>2</sup>) archival data with the project codes AM0601, AM577, AP0501. These data have a variety of array configurations (A-, B-, C-, and CD-array) and frequencies (1.4–43 GHz). The VLA A- and C-array data at 1.4 GHz (AP0501) are (probably) the same as Antón et al. (2008) previously presented. More improved images are reported in the present paper.

Data reduction was performed using the Astronomical Image Processing System (AIPS; Greisen 2003) in accordance with the standard procedures for the VLA continuum observation. Final calibrations were performed by CLEAN deconvolution and self-calibration iteratively using the software *difmap* (Shepherd et al. 1994). We found several radio sources with significant flux contributions in the primary beam of the VLA ( $\sim 30'$  at 1.4 GHz) around 1H 0323+342. We carefully modeled them by the CLEAN procedure for subsequently iterations of self-calibration. Radio images, in particular at 1.4 GHz, have significantly improved through the rejection of the contaminating emission. We display final images for each array configuration at 1.4 GHz with natural weighting (Figure 1). We define the names of components, K0, K1, K2, NE, and SW, as denoted in these images.

A combined VLA A+B+C-array image at 1.4 GHz was also made (Figure 2). After combining all the 1.4-GHz data, each of which was separately preprocessed by self-calibration and subtracting model visibilities of central sources (K0, K1, and K2), we restored visibilities of central components that had been constructed from the A-array data to the combined data, and then made an image via *tclean* in the Common Astronomy Software Applications (CASA) package (McMullin et al. 2007). As the result of several trials, we applied Briggs’s clean with robust = 0 (Briggs 1995) and beam restoring of  $3''$ . The NE region seen in the C-array image were resolved into substructures, named NE0–NE3, as denoted in the combined image.

The images at the other higher frequencies (8.4–43 GHz; AM577) are not shown in this paper, because only a similar radio structure consists of K0, K1, and K2 was observed. Figure 3 shows a radio continuum spectrum for each component; the results of flux measurements are listed in Table 1.

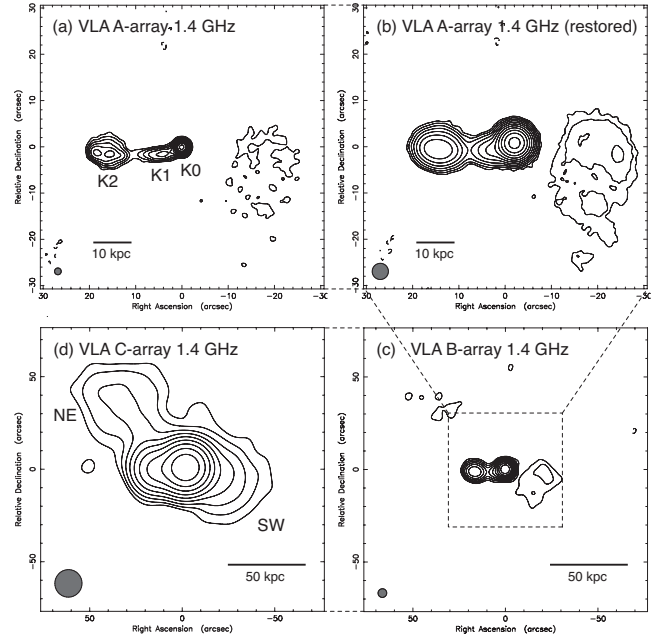


**Figure 1.** Radio images of 1H 0323+342 at kpc scales. Contour levels are separated by factors of 2 beginning at  $3\sigma$  of the rms image noise. Beam size is illustrated as a gray circle at lower left in each panel. (a) VLA A-array image at 1.4 GHz; (b) VLA A-array image convolved using a restored beam of  $3''.5$ ; (c) VLA B-array image at 1.4 GHz; (d) VLA C-array image. Component names in this paper are indicated in images (a), and (d): K0, K1, and K2 are of a VLA-scale core, a jet, and an inner lobe-like structure at kpc scales, respectively; SW and NE are of a south-west lobe and an north-east lobe as outermost components, respectively. The image noises are  $1\sigma = 0.09, 0.44$ , and  $0.33 \text{ mJy beam}^{-1}$  for A-, B-, and C-array images, respectively.

The error of flux density was determined from root-sum-square of the assumption for VLA flux scaling error (5% at 1.4–8.5 GHz and 10% at 15–43 GHz) and the source identification error in the Gaussian model fitting.

## 3 RESULTS

### 3.1 Radio morphology

The armed structure in the northeastern side can easily trace the evolution of jet’s position angle from the nucleus to the outermost region, while the emission in the south-western side exhibits an isolated ring-like structure rather than armed morphology (Figure 2). Significant asymmetry with respect to the nucleus is also apparent in terms of the maximum extent and brightness.

In the inner kpc region (Figure 1 (a)), we discovered a well-defined core–jet–lobe structure with edge-brightened morphology that is reminiscent of FR II radio galaxies. K0 and K1 are compact and narrow in width, while K2 is significantly resolved in the transverse direction of the jet flow. The structure elongates eastward with a curve, and reaches  $\sim 20''$  ( $\sim 24 \text{ kpc}$  in the projected distance) and is terminated at K2 in this image. The one-sided morphology indicates that the K0–K2 structure are in the approaching-jet side. K0 is a flat-spectrum core with a spectral index of

<sup>2</sup> The VLA is operated by the National Radio Astronomy Observatory, which is a facility of the National Science Foundation operated under cooperative agreement by Associated Universities, Inc.

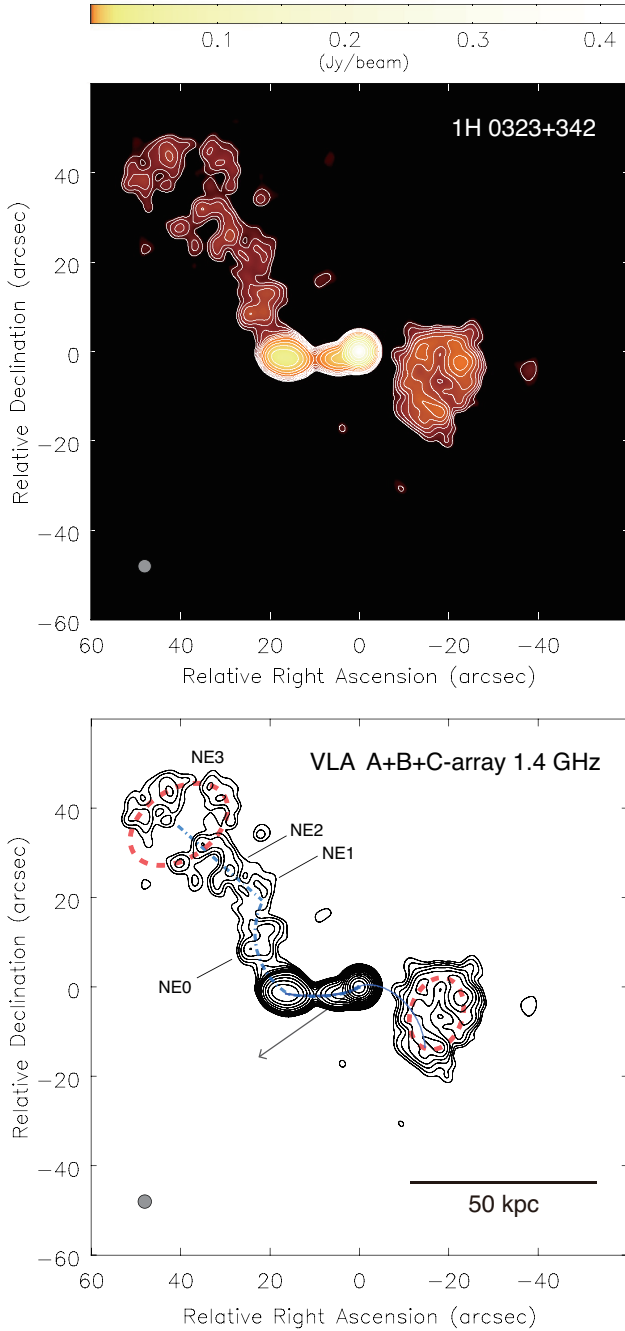


**Figure 2.** Combined VLA A+B+C-array image of 1H 0323+342 with a restoring beam of  $3''$ . Beam size is illustrated as a gray circle at lower left. Contour levels are  $3\sigma \times (-1, 1, \sqrt{2}, 2, 2\sqrt{2}, 4, 4\sqrt{2}, 8, 16, 32, \dots)$ , where  $\sigma (= 0.053 \text{ mJy beam}^{-1})$  is the image rms noise. (*Upper*) Radio-intensity map with intensity given by the color bar in units of  $\text{Jy beam}^{-1}$  and overlaid contours. (*Lower*) Contour map with descriptions/illustrations of radio components and structures. Substructures in NE are denoted by NE0–NE3. The arrow represents the position angle  $\text{PA} = 125^\circ$  for the pc-scale jet. Red dashed ellipses are traces of relic lobes (NE3 and SW). Blue curves represent one of solutions of the recently started precession model;  $\beta_{\text{inner}} = 0.65$ ,  $\beta_{\text{outer}} = 0$ , and  $P_{\text{prec}} = 2.5 \times 10^6 \text{ yr}$  (Section 4.3 and Table 2). The bold solid, bold dot-dashed, and thin solid curves represent the trajectories of the active jet-lobe, relics, and expected counter jet, respectively.

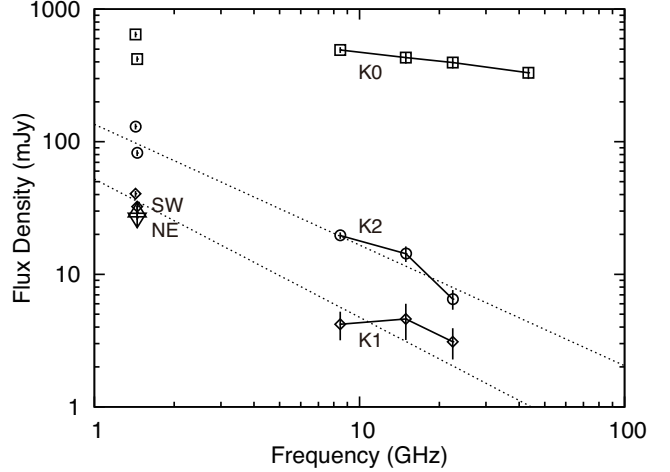


**Figure 3.** Radio continuum spectra of 1H 0323+342. Squares, diamonds, circles, upward triangle, and downward triangle represent measured flux densities of K0, K1, K2, SW, and NE, respectively. Symbols connected with solid lines represent quasi-simultaneous observations. Dotted lines represent fitted power-law spectra for K1 and K2.

$\alpha = -0.24 \pm 0.01$  at 8.4–43 GHz, where  $\alpha$  is the spectral index in  $S_\nu \propto \nu^\alpha$ ,  $S_\nu$  is the flux density at the frequency  $\nu$ . K1 and K2 are an optically-thin jet and a lobe showing steep spectra of  $\alpha = -1.04 \pm 0.16$  and  $-0.91 \pm 0.11$ , respectively (Figure 3).

The northeastern emission (NE) exhibits an outermost radio emitting region with an elongation up to  $\sim 60''$ , corresponding to  $\sim 72 \text{ kpc}$  in the projected distance. NE was not detected in the VLA a-array images (Figures 1 (a)–(b)), indicating very low brightness. We define sub-structures NE0–NE3 in NE on Figure 2; NE3 potentially shows ring-like morphology. NE1–NE2–NE3 are well-aligned at a position angle of  $\sim 48^\circ$  from the core K0, which is quite different from the position angles of the inner FR II-like structure. NE0 is seen as a bridging emission between the K2 lobe and NE1. Hence, NE is in the approaching-jet side. No hotspot-like feature is seen in the NE region.

The southwestern emission (SW) in low brightness (Figure 1 (d)) has been resolved into an isolated emitting region in high-angular-resolution images (Figures 1 (b) and (c)). In the combined image (Figure 2), sub-structures in SW have been revealed to be shell-like morphology. Therefore, SW and NE3 apparently form a pair of the outermost lobes. We cannot find evidence for the centrosymmetric counterpart corresponding to the jet-lobe structure K1–K2. No bridging emission as a counter jet connecting with SW was detected. The total flux density of SW nearly equals to that of NE (Table 1). On the other hand, the asymmetry of the NE–SW morphology is ascribable to the smaller separation distance and higher brightness of SW than those of NE.

Previously, Antón et al. (2008) presented VLA A- and C-array images at 1.4 GHz, which originated in archival data (probably) the same as we used (AP0501; Figure 1 (a) and (d)), and only brief discussions for the radio structure. Two-sided radio morphology was also pointed out by Antón et al. (2008) based on their C-array image. However, NE component was not detected in their A-array image. The emitting region NE and the internal structures in NE and SW have



**Table 1.** Observation data and results of flux density measurements

Project	Array	$\nu$ (GHz)	$S_\nu$ (mJy)	Comp.
(1)	(2)	(3)	(4)	(5)
AM0601	VLA-B	1.43	$645.3 \pm 32.3$	K0
			$40.5 \pm 2.1$	K1
			$130.2 \pm 6.5$	K2
AM577	VLA-CD	8.46	$491.7 \pm 24.6$	K0
			$4.2 \pm 0.5$	K1
			$19.6 \pm 1.1$	K2
		14.96	$431.6 \pm 43.2$	K0
			$4.6 \pm 1.4$	K1
			$14.3 \pm 1.9$	K2
		22.49	$396 \pm 39.6$	K0
			$3.1 \pm 0.8$	K1
			$6.5 \pm 1$	K2
AP0501	VLA-A	1.45	$330.8 \pm 33.7$	K0
			$32.4 \pm 1.8$	K1
			$82.2 \pm 4.2$	K2
AP0501	VLA-C	1.45	$26.7 \pm 3.5$	NE
			$29.3 \pm 3.6$	SW

Note. — Column 1: project code; Column 2: telescope array; Column 3: center frequency; Column 4: flux density; Column 5: component name.

been first identified in our study. We point out the FR II-like morphology of K1–K2 for the first time. These findings may be ascribable to the improved quality of our images by a careful treatment of contamination sources outside of the field of view (Section 2).

### 3.2 The Position-angle profile of radio structures

Figure 4 is the plot tracing the jet structure in position angles with a dependence on the angular distance from the nucleus in the approaching-jet side. K1 was reproduced with five sub-components using `modelfit` in `difmap` on Figure 1 (a). NE0–NE2 were identified using `imfit` in `CASA`. The position of NE3 is the center of a fitted elliptical. The pc-scale jet of 1H 0323+342 is being ejected toward the position angle  $PA \sim 125^\circ$  in VLBI images (Wajima et al. 2014; Fuhrmann et al. 2016; Doi et al. 2018; Hada et al. 2018). On the other hand, the outermost radio structure NE1–NE3 extends at  $PA = 48^\circ \pm 1^\circ$ , quite different from that of pc-scale jet. The NE1–NE3 structure is also well-aligned toward the nucleus.

The K0–K1–K2 radio structure is curved, and its position angle changes progressively from  $PA \sim 120^\circ$  to  $\sim 95^\circ$ . The upstream of K1 connects with the pc-scale jet smoothly, while the outermost radio structure NE1–NE3 is not on the extension of the trend of the K0–K1–K2 structure. NE0 bridges between K2 and NE1.

It was difficult to trace the distance-dependent structure on the counter side. The center of the SW lobe is located at  $PA \sim -109^\circ$ , which is slightly misaligned by  $\sim 21^\circ$  with that of NE3 lobe.

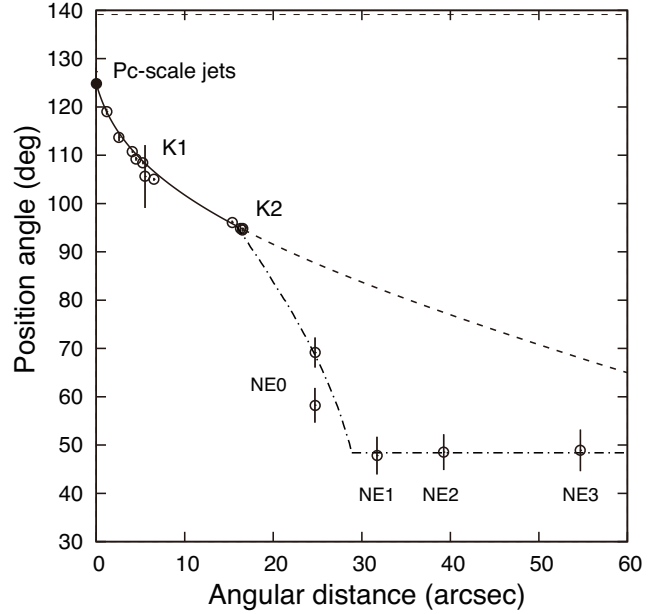


**Figure 4.** Plot of position angle vs. angular distance on approaching-jet side. Open symbols represent measurements on VLA images at 1.4–8.4 GHz. A filled symbol at  $(0''007, 125^\circ)$  represents the position angle of pc-scale jets. Solid and dashed curves represent an expected trajectory by a precession model as an example ( $\beta_1 = 0.7$  and  $P_{\text{prec}} = 2.8 \times 10^6$  yr; Section 4.1); note that this example is not a unique solution. A dot-dashed curve and a line represent an alternative expected trajectory for a precession + deceleration model, which assumes a lower speed ( $\beta_2 = 0.15$ ) in the outer region as a head speed of the radio lobe.

## 4 DISCUSSION

Key findings of the present study are (1) a one-sided, FR II-like jet–lobe structure at the inner kpc-scale emission (K1–K2), (2) misalignments in the position angles among the pc-scale jet, the FR II-like inner kpc-scale structure with a curve, and an outermost low-brightness radio lobe (NE), and (3) a spatially identified low-brightness radio emitting region (SW) on the counter-jet side. We discuss the possible origin of the apparently peculiar radio morphology in 1H 0323+342.

### 4.1 The origin of anomalous radio morphology

Overall radio morphology of the  $\gamma$ -NLS1 1H 0323+342 is reminiscent of X-shaped radio galaxies (e.g., Murgia et al. 2001) but exhibits significant asymmetry. X-shaped radio galaxies usually consist of a pair of FR II radio arms with active lobes (“primary lobes”) and a pair of lower-brightness lobes with no hotspots (“secondary lobes” or “wings”). In the case of 1H 0323+342, the inner FR II-like radio structure K1–K2 is interpreted as a primary lobe, and the outermost emitting region NE is as the secondary lobe. In this scenario, the primary lobes should be currently energized by the active nucleus. The inner structure is apparently one-sided, which is consistent with the existence of a jet and an undetectable counter-jet due to Doppler boosting/de-boosting (discussed later in Section 4.3). On the other hand, NE exhibit very low-brightness and no hotspots. It is likely that the NE region

is no longer energized by the central engine and a relic as the past jetted activity. An armed structure is not obvious in the counter-jet side, but the emitting region SW certainly appears in a corresponding opposite range of position angles (between  $\sim -80^\circ$  and  $\sim -135^\circ$ ; Figure 2).

The physical origin of the X-shaped radio galaxies may be discussed in the framework of (1) the spin-flip scenario, (2) hydrodynamic effects, and (3) the precession model. The spin-flip scenario postulates a change of the jet direction due to a sudden flip of black hole’s spin axis through a coalescence with another black hole in a minor merger (e.g., Merritt & Ekers 2002). The scenario predicts (i) a rapid change of jet direction, (ii) reorientation only once, and (iii) a stable jet axis after the event. The spin-flip scenario cannot be applied to the case of 1H 0323+342, because of the observed curved jet structure (K1) up to the active lobe and the presence of transitional structure (NE0) between the position angles of the primary and secondary lobes; the observed structure rather indicates an ongoing gradual reorientation. The hydrodynamic effects as an interaction with the surrounding interstellar medium (ISM; the backflow diversion model (e.g., Leahy & Williams 1984; Capetti et al. 2002) have also been discussed. In this framework, the jet-shell interaction model (Gopal-Krishna et al. 2012)) have been proposed for cases where the “Z-symmetric” morphology is apparent in secondary lobes. For 1H 0323+342, this mechanism is unlikely because of the straight propagation in the outermost structure of NE1–NE3, which is also well-aligned toward the nucleus. NE1–NE3 are presumably the oldest radio structures, but show no evidence of the experience of hydrodynamical distortion.

The precession model is consistent with at least the inner part of radio morphology, which exhibits the smoothly curved structure throughout the pc-scale jet, the edge-brightened jet-lobe (K1–K2), and the transitional emission NE0. The warping instability of an accretion disc (Pringle 1996) would explain a precessing jet direction; however, it is a stochastic rather than a regular precession. Alternatively, a precessing jet can also be present in the case of a binary blackhole system formed via a merger (e.g., Begelman et al. 1980; Liu & Chen 2007). In the case of 1H 0323+342, previous work has shown that this object hosts a perturbed galaxy, that might have resulted from a merging process (Antón et al. 2008; León Tavares et al. 2014). Hence, we conclude that the model of precessing jet of a binary black hole system is most preferable to explain the origin of the anomalous radio morphology in 1H 0323+342.

#### 4.2 Timescales of the galaxy merger and jet activity

The optical image of the host galaxy of 1H 0323+342 exhibits colour gradient profiles inside and across the off-centered ring structure that is very similar to those detected in collisional ring galaxies with star formation (Antón et al. 2008). The timescales of ring formation ( $\sim 50$  Myr; Mapelli & Mayer 2012) and star-forming clumps in interacting and merging systems ( $\sim 10$  Myr; Hancock et al. 2007) can be considered for the age as a merger system for 1H 0323+342.

Meanwhile, it takes a considerable amount of time from the start of a galactic merger to the formation of a black hole

binary. The dynamical friction timescale where the captured black hole sinks to the central region of the galaxy is  $t_{\text{sink}} \sim 2 \times 10^8 \text{ yr } (\sigma_*/200 \text{ km s}^{-1})^5 (m/10^7 M_\odot)^{-3/4}$ , where  $\sigma_*$  is the stellar velocity dispersion and  $m$  is the mass of the captured black hole (Merritt & Ekers 2002). For a black hole mass of  $M = 3.4 \times 10^7 M_\odot$  for 1H 0323+342 (Wang et al. 2016)  $\sigma_* \approx 120 \text{ km s}^{-1}$  is expected from an empirical relation  $M \approx 0.309 \times (\sigma_*/200 \text{ km s}^{-1})^{4.38} 10^9 M_\odot$  (Kormendy & Ho 2013). As a result,  $t_{\text{sink}} \sim 10\text{--}80$  Myr if we assume  $m/M \sim 1/3\text{--}1/30$  as a typical minor major. Thus, this estimated timescale is consistent with the merger age of 1H 0323+342.

Such a large time scale for the formation of binary black hole system means that a significantly large radio structure can be formed before the start of jet precession. The outermost radio emitting region consisting of NE1–NE3 shows a straight morphology, which is well-aligned toward the nucleus, up to 72 kpc in projected distance; no signature of distortion by jet precession are seen in this outermost structure. Assuming a typical advancing speed of  $\sim 0.01c\text{--}0.1c$  for the head of FR II radio lobes (Kawakatu et al. 2008, and references there in), the estimated age of the radio relic NE3 is roughly 10–100 Myr (assuming a viewing angle of  $\sim 10^\circ$ ; Section 4.3), which is consistent with the possible timescale of the galaxy merger in 1H 0323+342 as discussed above. Hence, the jet activity of 1H 0323+342 might have started triggered by the galaxy merger. A large fraction of radio-loud AGNs are associated with recent or ongoing merger events (Ramos Almeida et al. 2012; Chiaberge et al. 2015), which is a strong indication that mergers are the triggering mechanism for the launching of relativistic jets from SMBHs.

On the other hand, the curved structure K1–K2 up to 24 kpc in the projected distance can be considered as a jet recently formed after the binary system had been established and the precession started. The apparent one-sidedness of the K1 jet implies the Doppler beaming effect. The jet-to-counter jet intensity ratio  $R_1 > 69$  (Eq. A2, the ratio of a peak intensity of 11 mJy beam $^{-1}$  in the K1 jet to three times the image noise  $\sigma = 0.053$  mJy beam $^{-1}$  (Figure 2)), constrains the jet speed  $\beta > 0.61$  in the units of speed of light. This leads to an upper limit of the kinematic age of K2,  $\lesssim 1$  Myr, if we adopt a viewing angle of  $3^\circ$  (Abdo et al. 2009).

Therefore, the anomalous radio structure of 1H 0323+342 presumably contains traces of the history of jet activity both before and after the formation of a binary black hole system.

#### 4.3 A recently started jet precession model

In this subsection, we present a toy model of jet precession that started from the formation of a binary SMBH system long after a galaxy merger. Possible timescales and geometric parameters are provided by this model for the observed radio morphology in 1H 0323+342.

We initially attempted to reproduce the profile of the approaching-jet side with a simple precession model (Caproni & Abraham 2004) that assumes ballistic jets with a constant speed and a constant precession pitch. The set of parameters are the jet speed  $\beta$  in the unit of speed of light, the semi-aperture angle of the precession cone  $\Omega$ , the angle between the precession cone axis and the line of sight  $\phi_0$ , and the period of precession  $P_{\text{prec}}$ . We searched parameters under constraints of (i)  $\beta > 0.61$  and (ii) the current viewing

**Table 2.** Parameters of recently started jet precession model

Case	$\theta_{\text{pc}}$ (deg)	$\Omega$ (deg)	$\phi_0$ (deg)	$P_{\text{prec}}$ (yr)	$t_{\text{start}}$ (yr)	$\theta_{\text{NE1--NE3}}$ (deg)	$t_{\text{K2}}$ (yr)	$\theta_{\text{K2}}$ (deg)
(1)	(2)	(3)	(4)	(5)	(6)	(7)	(8)	(9)
$\beta_{\text{inner}} = 0.65, \beta_{\text{outer}} = 0$	3	7.3	6.4	$2.5 \times 10^6$	$8.8 \times 10^5$	13	$2.7 \times 10^5$	7.2

Note. — Column 1: the case of jet speeds in the inner and outer kpc scales. We found good solutions from cases of  $0.61 < \beta_{\text{inner}} \lesssim 0.7$ ,  $\beta_{\text{outer}} \sim 0$ ; Column 2: assumed viewing angle at the pc scale; Column 3: the semi-aperture angle of the precession cone; Column 4: the angle between the precession cone axis and the line of sight; Column 5: the period of precession; Column 6: time from precession start; Column 7: the viewing angle of NE1–NE3; Column 8: the age of K2; Column 9: the viewing angle of K2.

angle  $\theta_{\text{pc}} = 3^\circ$ . The first constraint comes from the apparent one-sidedness of the K1 jet (Section 4.2). The second constraint comes from the spectral-energy-distribution modeling including the  $\gamma$ -ray regime for 1H 0323+342 (Abdo et al. 2009); this viewing angle is consistent with the detection of superluminal motion of  $\beta_{\text{app}} = 9.0 \pm 0.3$  in the pc-scale jet (Lister et al. 2016).

We obtained good results in the fit to the currently active jet, namely from the pc-scale jet to the outer tip of the K2 lobe (the solid curve in Figure 4), but, failed in the fit over the entire angular scales with any combinations of parameters (the dashed curve in Figure 4). Note that because of only a limited number of measurements we had to fix the jet speed  $\beta$  to determine the rest of precession parameters  $P_{\text{prec}}$ ,  $\Omega$ , and  $\phi_0$ . Almost the same trajectories on the sky plane were obtained with various values of  $0.61 < \beta \lesssim 1$ . However, NE components were largely deviated from the model curves. In the cases of  $\beta \gtrsim 0.70$  the expected trajectory in the counter-jet side cannot reach the distance of SW region in a single precession cycle, because of huge asymmetry due to the light-travel-time effect (Eq. (A1)). Hence, we postulate that the jet has become sub-relativistic ( $0.61 < \beta \lesssim 0.70$ ) from the highly relativistic ( $\beta \sim 0.995$ , e.g., (Fuhrmann et al. 2016)) before escaping the pc-scale region.

Next, we modified the precession model by introducing (a) different advancing speeds in the inner and outer distances and (b) a start time of the precession. This step-wise speed profile was intended to switch from a high speed ( $\beta_{\text{inner}}$ ) to a low speed ( $\beta_{\text{outer}}$ ) at a boundary distance from the nucleus. The former modification provided a good result to reproduce the bridging structure of K2–NE0–NE1, when  $\beta_{\text{outer}} \sim 0$  ( $< 0.1$ ). This means that the position angle of the shock front changes gradually, while the bulk of accelerated synchrotron electrons stay behind at the same position angle. This is a similar approach applied to the structure between the active lobe and the tail of wings in X-shaped radio galaxies (Gong et al. 2011). By the later modification, before the precession started, we consider that the shock front was continuously supplied with kinetic energy through the jet at  $PA = 48^\circ$  to form the linear structure that extends further away (NE1–NE3). Consequently, this recently-started precession model including a deceleration is well-reproduced the NE structure as shown in dot-dashed curve/line in Figures 2 and 4). Table 2 lists the determined parameters for the case of  $\beta_{\text{inner}} = 0.65$  as representative case. For the cases  $0.61 < \beta \lesssim 0.70$ , determined parameters were very similar.

In this scenario, the jet speed was  $\beta_{\text{inner}} \sim 0.6$ – $0.7$  in

the inner kpc region, and has changed to  $\beta_{\text{outer}} \sim 0$  at a distance where the outer tip of the K2 lobe is observed. The jet initially directed to  $PA \sim 48^\circ$  and a viewing angle of  $\theta_{\text{NE1--NE3}} \sim 13^\circ$  and formed the NE1–NE3 structure of linear morphology; a precession started  $t_{\text{start}} \sim 1$  Myr ago with the period of precession  $P_{\text{prec}} \sim 3$  Myr, the position angle of the hotspot gradually moved and NE0 was left out as a relic; the kinematic age of the currently observed K2 lobe is  $t_{\text{K2}} \sim 0.3$  Myr (at the viewing angle  $\theta_{\text{K2}} \sim 7^\circ$ ) in the observer frame. The precession continues today as jet’s viewing angle decreases ( $\theta_{\text{pc}} = 3^\circ$  at the pc scale) and 1H 0323+342 is detected in  $\gamma$ -rays.

By using  $P_{\text{prec}} \sim 600(r/10^{16}\text{cm})^{5/2}(M/m)(M/10^8 M_\odot)^{-3/2}\text{yr}$  (Begelman et al. 1980) and assuming a typical minor merger ( $m \sim 0.1M$ ), an orbital radius of  $\sim 0.05$  pc is estimated, which is far from the range where the orbit is effectively shrunk via gravitational radiation. The central engine of 1H 0323+342 may be currently in the intermediate stage of a binary black hole system. We tried to detect the expected winding structure in the pc-scale jet in the series of very-long-baseline interferometry (VLBI) images<sup>3</sup> of 1H 0323+342 during our previous study (Doi et al. 2018). However, no significant sign beyond measurement errors was detected because the expected amplitude 0.05 pc corresponding to 0.04 milli-arcsecond (mas) was too small in the jet extending to about 10 mas.

#### 4.4 Relics as a reservoir of past jet powers

NE0–NE3 seen far from the edge-brightened active lobe K2 was found in very low brightness, and the outermost region NE3 shows no clear evidence of a hotspot. Hence, NE0–NE3 are no longer energized by the nucleus through jets and is therefore left as radio relics on the approaching-jet side.

SW exhibits shell-like morphology with low brightness without armed structures, and is likely to form outermost paired lobes with NE3 that also shows a ring-like structure (Figure 2). The northern part of SW ( $PA \sim -85^\circ$ ) looks as if it were a counter lobe corresponding to K2, because roughly a comparable separation ( $\sim 20''$ ) was observed on each side. However, we can rule out the possibility, because the light-travel-time effect (Eq. (A4)) postulates a much less arm length of  $< 8''$  in the counter-jet side in the case of the

<sup>3</sup> We used VLBI images obtained at 15.3 GHz in the Monitoring of Jets in AGNs with very long baseline array (VLBA) experiments (MOJAVE; Lister & Homan 2005)

jet speed  $\beta > 0.61$  (Eq. (A1)). Moreover, the total flux density of SW nearly equals to that of NE, which indicates that the advancing speeds of the both lobes have been decelerated to  $\beta \sim 0$  in the framework of Doppler beaming effect (the flux density ratio  $R_F \sim 1$ , Eq. (A3)). Hence, the whole emission of SW can be interpreted as a relic on the counter-jet side.

The paired relic of NE/SW exhibits highly asymmetric morphology in terms of the maximum extent, brightness, and position angle. The arm-length ratio of  $R_L \sim 60''/25''$  (Eq. (A1)) cannot make a compromise with the flux density ratio  $R_F \sim 1$  (Eq. (A3)) even at any possible values of the jet speed  $\beta$  and viewing angle  $\theta$ . In addition, significantly higher surface brightness in the counter-jet side (SW) compared to the approaching side (NE). Such properties are possibly caused by jet interactions with an inhomogeneous ISM (e.g., Gopal-Krishna & Wiita 2004). In the SW region, the same amount of jet kinetic energy may be confined in a cavity smaller than the NE region. The misalignment by  $PA \sim 21^\circ$  between the centers of SW's and NE3's elliptical outlines is also ascribable to the interaction in surrounding environments that is asymmetric on approaching- and counter-jet sides.

Using the relation between the radio luminosity and the cavity power in X-ray-emitting hot gas (Cavagnolo et al. 2010), we estimated the kinetic power of lobes NE and SW to be  $\sim 10^{43.7}$  ergs  $s^{-1}$ , which is comparable with or slightly less than an estimate for the innermost jet that emits  $\gamma$ -rays ( $10^{44}$ – $10^{45}$  ergs  $s^{-1}$ ; Paliya et al. 2014). This relatively large power suggests that the past jet activity also had sufficient jet kinetic powers for escaping to kpc scales in the form of supersonic lobes, which make FR II morphology (Kawakatu et al. 2009).

Edge-brightened, FR II-like radio morphology at kpc scales has been evidently discovered in a fraction of radio-loud NLS1s: PKS 0558-504 (Gliozzi et al. 2010), FBQS J1644+2619 (Doi et al. 2011, 2012), SDSS J120014.08-004638.7 (Doi et al. 2012, J0953+2836, J1435+3131, J1722+5654 (Richards & Lister 2015), J0814+5609 (Berton et al. 2018), SDSS J103024.95+551622.7 (Rakshit et al. 2018; Gabányi et al. 2019), while an FR I-like one has been found in the radio-quiet/intermediate NLS1 (Mrk 1239, Doi et al. 2015). These FR II-like structures extend up to  $\sim 10$ – $100$  kpc in the projected size, indicating that supersonic jet flows with sufficiently large jet kinetic powers are emanated from the NLS1 central engines even with low masses of SMBHs, in addition to evidence for the long-lasting ( $\gtrsim 10^7$  yr) FR II jet activity (Doi et al. 2012). Thus, 1H 0323+342 in the present study is similar to these radio-loud NLS1s with FR II-like radio morphology in terms of the jet power and the age of jet activity (Section 4.2).

In these radio-loud NLS1s, significantly curved radio structure on their one side are seen in some cases (FBQS J1644+2619, J1435+3131, and J0814+5609), although well-aligned paired lobes at opposite directions are mostly observed. Interestingly, the brightest knot appears at the middle of a radio arm that also exhibits lower-brightness radio emission at the outermost region (J1435+3131 and J0814+5609). Such an arrangement is similar to the combination of K2 (the inner active lobe) and NE (the outer relic) in 1H 0323+342. These outermost emissions might be

relics abandoned due to the historical change of jet direction by precessions in binary black holes or flips of black hole's spin axis through coalescences in galaxy merger processes. Further researches are demanded in the future.

#### 4.5 Implications of 1H 0323+342 for the evolution of SMBHs and galaxies

Our radio observations has provided insight that 1H 0323+342 is associated with a merging system, from a different approach based on the distorted jet morphology. The result is supporting the previously reported signs of a recent violent dynamical interaction based on optical/near-infrared observations (Zhou et al. 2007; Antón et al. 2008; León Tavares et al. 2014; Olguín-Iglesias et al. 2020). The anomalous radio morphology, in which inner curved structures of the FR II-like jet and the outer linear structure of relics coexist (Section 3), is indicative of the stage of an precessing black hole binary before the black holes coalesce in the galaxy merger process on the radio-loud NLS1 1H 0323+342 (Sections 4.1 and 4.2).

On the other hand, the Sérsic index based on the surface-brightness analysis for the host galaxy suggests the presence of a pseudobulge (Olguín-Iglesias et al. 2020; see also León Tavares et al. 2014), which is thought to be developed through internal secular evolution with little experience of galaxy mergers. Therefore, 1H 0323+342 is a peculiar AGN, which conflicts with the relativistic-jet paradigm that radio-loud AGNs are exclusively associated with very high mass SMBHs in elliptical hosts, which is thought to be built-up through mergers.

Importantly, 1H 0323+342 is not the only radio-loud NLS1 associated with a pseudobulge. Kotilainen et al. (2016) have discovered a pseudobulge in the host galaxy of the  $\gamma$ -ray-emitting NLS1 PKS 2004-447. Olguín-Iglesias et al. (2017) found a barred lenticular morphology with a pseudobulge and a minor merger sign in the  $\gamma$ -ray-emitting NLS1 FBQS J1644+2619 (cf. D'Ammando et al. 2017). Olguín-Iglesias et al. (2020) reported the signs of disk (pseudo) bulges in many radio-loud NLS1s. These examples suggest the powerful relativistic jets can be launched from engines of low-mass SMBHs in pseudobulges, which challenges the conventional paradigm.

Interestingly, the black hole mass of 1H 0323+342 is  $3.4 \times 10^7 M_\odot$  based on reverberation mapping (Wang et al. 2016), which is certainly much lower compared to typical radio-loud AGNs, but at the high-mass end of the NLS1 population. Similarly, other radio-loud NLS1s also have relatively larger mass black holes (Komossa et al. 2006; Doi et al. 2012). This trend is partly approaching the relativistic-jet paradigm in the sense that relatively large mass black holes are preferentially present in radio-loud objects in the NLS1 population. Additionally, unlike radio-quiet NLS1s, the sign of galaxy interaction is frequently associated with radio-loud NLS1s (Olguín-Iglesias et al. 2020) including 1H 0323+342. On the hypothesis that a merger triggers jet activity (Chiaberge et al. 2015; Ramos Almeida et al. 2012), it is likely that these radio-loud NLS1s became radio-loud from radio-quiet AGNs in the NLS1 population. Thus, 1H 0323+342 and other radio-loud NLS1s in pseudobulges under galaxy interactions might be



extreme NLS1s on a way of the evolutionary track to normal Seyferts with larger SMBHs and classical bulges.

## 5 CONCLUSION AND SUMMARY

The host galaxy of the radio-loud  $\gamma$ -ray-emitting NLS1 1H 0323+342 exhibits a combination of the two contradictory signs, a disturbed morphology due to a recent merger and a pseudobulge suggestive of internal secular evolution with little merger experience before. In the present study, we presented detailed investigations of the distorted radio morphology associated with 1H 0323+342. The precession may be attributed to the binary black hole system, which were recently formed by capturing the secondary black hole through the merger process. The observed peculiar radio morphology is interpreted as the result of changes in the direction of black hole's spin axis, in a framework in which a binary black hole system is formed via a merger process. Thus, 1H 0323+342 is an example among radio-loud NLS1s in pseudobulges under galaxy interactions, which might be extreme NLS1s on a way of the evolutionary track from radio-quiet NLS1s to AGNs with larger SMBHs and classical bulges. The conclusion have been made by following summary of our investigations based on radio imaging for 1H 0323+342:

- We made radio images at frequencies of 1.4–43 GHz from VLA archival data. At 1.4 GHz, detailed radio structures of 1H 0323+342 has been revealed from the combined data obtained with A-, B-, and C-array configurations.
- The inner kpc-scale jet shows a one-sided, jet-lobe structure terminated at  $\sim 20''$  (corresponding to  $\sim 24$  kpc in projected size) from the nucleus, and exhibits an FR II-like edge-brightened radio morphology. This radio structure is curved, smoothly connected with the pc-scale jets, and therefore, currently energized by the central engine.
- In the further outside, a low-brightness radio emitting region is distributed linearly up to  $\sim 60''$  ( $\sim 70$  kpc in projected size) at a position angle significantly different from those of the inner kpc-scale structure and pc-scale jet. A low-brightness component in the counter-jet side was also identified, and is separated without the bridging structure from the nucleus. The two outermost components are almost equal in flux density, indicating substantially decelerated in advancing speeds. These outer components are left as relics of past jet activities.
- The precessing binary black hole scenario in the framework of X-shaped radio galaxies is most preferable to explain the anomalous radio morphology. It potentially took a significant time for dynamical friction to establish the binary black hole system ( $\sim 10$ – $80$  Myr) from the beginning of the galaxy interaction. This timescale is comparable to a possible kinematic age of the outermost radio component ( $\sim 10$ – $100$  Myr). The jet activity might be triggered by a merger event. The estimated kinematic age of the inner jet-lobe structure with a curve trajectory is only  $\sim 1$  Myr. Precession may have started when the binary black hole system was established at the galactic center.
- We presented a possible solution in a recently-started jet precession model. The pc-scale and inner kpc-scale jets with a curve (K1–K2) was fitted well with a simple precession model. The base of jet is now almost pole-on viewed.

The low-brightness bridging emission (NE0) can also be reproduced as a relic on the precession trajectory of the shock front. The outermost low-brightness linear structure (NE1–NE3) is considered as a relic linearly expanded to the initial direction without precession.

## ACKNOWLEDGMENTS

The Karl G. Jansky Very Large Array is operated by the National Radio Astronomy Observatory, which is a facility of the National Science Foundation operated under cooperative agreement by Associated Universities, Inc. This work was partly supported by JSPS KAKENHI Grant Numbers JP18K03656(MK), JP18H03721(MK), JP19K03918(NK), and JP20K04020(AD).

## APPENDIX A: DOPPLER BEAMING EFFECT AND LIGHT-TRAVEL-TIME EFFECT

If we consider jets of a ballistic motion with a same constant advancing speed on the both side and a same intrinsic intensity/flux density on the both side. The apparent arm length ratio ( $R_L$ ), the observed intensity ratio ( $R_I$ ), the observed flux density ratio ( $R_F$ ) of an approaching and receding jet, and the apparent jet velocity  $\beta_{\text{app}}$  are expressed as (e.g., Ghisellini et al. 1993; Gopal-Krishna & Wiita 2004)

$$R_L = \frac{1 + \beta \cos \theta}{1 - \beta \cos \theta}, \quad (\text{A1})$$

$$R_I = \left( \frac{1 + \beta \cos \theta}{1 - \beta \cos \theta} \right)^{2-\alpha}, \quad (\text{A2})$$

$$R_F = \left( \frac{1 + \beta \cos \theta}{1 - \beta \cos \theta} \right)^{3-\alpha}, \quad (\text{A3})$$

$$\beta_{\text{app}} = \frac{\beta \sin \theta}{1 - \beta \cos \theta}, \quad (\text{A4})$$

where  $\beta$  is the jet speed in the unit of speed of light,  $\theta$  is the viewing angle.

## REFERENCES

- Abdo A. A., et al., 2009, *ApJ*, **707**, L142  
 Antón S., Browne I. W. A., Marchã M. J., 2008, *A&A*, **490**, 583  
 Bagchi J., et al., 2014, *ApJ*, **788**, 174  
 Begelman M. C., Blandford R. D., Rees M. J., 1980, *Nature*, **287**, 307  
 Berton M., et al., 2018, *A&A*, **614**, A87  
 Berton M., et al., 2019, *The Astronomical Journal*, 157, 48  
 Briggs D. S., 1995, in *American Astronomical Society Meeting Abstracts*. p. 1444  
 Capetti A., Zamfir S., Rossi P., Bodo G., Zanni C., Massaglia S., 2002, *A&A*, **394**, 39  
 Caproni A., Abraham Z., 2004, *MNRAS*, **349**, 1218  
 Cavagnolo K. W., McNamara B. R., Nulsen P. E. J., Carilli C. L., Jones C., Birzan L., 2010, *ApJ*, **720**, 1066  
 Chiaberge M., Gilli R., Lotz J. M., Norman C., 2015, *ApJ*, **806**, 147  
 Crenshaw D. M., Kraemer S. B., Gabel J. R., 2003, *AJ*, **126**, 1690  
 D’Ammando F., Acosta-Pulido J. A., Capetti A., Raiteri C. M., Baldi R. D., Orienti M., Ramos Almeida C., 2017, *MNRAS*, **469**, L11

- D’Ammando F., Acosta-Pulido J. A., Capetti A., Baldi R. D., Orienti M., Raiteri C. M., Ramos Almeida C., 2018, *MNRAS*, **478**, L66
- Davis B. L., Graham A. W., Cameron E., 2019, *ApJ*, **873**, 85
- Deo R. P., Crenshaw D. M., Kraemer S. B., 2006, *AJ*, **132**, 321
- Doi A., Asada K., Nagai H., 2011, *ApJ*, **738**, 126
- Doi A., Nagira H., Kawakatu N., Kino M., Nagai H., Asada K., 2012, *ApJ*, **760**, 41
- Doi A., Wajima K., Hagiwara Y., Inoue M., 2015, *ApJ*, **798**, L30
- Doi A., Hada K., Kino M., Wajima K., Nakahara S., 2018, *ApJ*, **857**, L6
- Ferrarese L., Merritt D., 2000, *ApJ*, **539**, L9
- Fisher D. B., Drory N., 2008, *AJ*, **136**, 773
- Fuhrmann L., et al., 2016, *Research in Astronomy and Astrophysics*, **16**, 176
- Gabányi K. É., Frey S., Veres P., Moór A., 2019, arXiv e-prints, Gebhardt K., et al., 2000, *ApJ*, **539**, L13
- Ghisellini G., Padovani P., Celotti A., Maraschi L., 1993, *ApJ*, **407**, 65
- Giozzi M., Papadakis I. E., Grupe D., Brinkmann W. P., Raeth C., Kedziora-Chudczer L., 2010, *ApJ*, **717**, 1243
- Gong B. P., Li Y. P., Zhang H. C., 2011, *ApJ*, **734**, L32
- Gopal-Krishna Wiita P. J., 2004, ArXiv Astrophysics e-prints, Gopal-Krishna Biermann P. L., Gergely L. Á., Wiita P. J., 2012, *Research in Astronomy and Astrophysics*, **12**, 127
- Graham A. W., Scott N., 2015, *ApJ*, **798**, 54
- Greisen E. W., 2003, *Information Handling in Astronomy - Historical Views*, **285**, 109
- Hada K., et al., 2018, *ApJ*, **860**, 141
- Hancock M., Smith B. J., Struck C., Giroux M. L., Appleton P. N., Charmandaris V., Reach W. T., 2007, *AJ*, **133**, 676
- Hopkins P. F., Hernquist L., Cox T. J., Kereš D., 2008, *ApJS*, **175**, 356
- Hota A., et al., 2011, *MNRAS*, **417**, L36
- Järvelä E., Lähteenmäki A., Berton M., 2018, *A&A*, **619**, A69
- Kawakatu N., Nagai H., Kino M., 2008, *ApJ*, **687**, 141
- Kawakatu N., Kino M., Nagai H., 2009, *ApJ*, **697**, L173
- Keel W. C., White Raymond E. I., Owen F. N., Ledlow M. J., 2006, *AJ*, **132**, 2233
- Kellermann K. I., Sramek R., Schmidt M., Shaffer D. B., Green R., 1989, *AJ*, **98**, 1195
- Komossa S., Voges W., Xu D., Mathur S., Adorf H.-M., Lemson G., Duschl W. J., Grupe D., 2006, *AJ*, **132**, 531
- Kormendy J., Ho L. C., 2013, *ARA&A*, **51**, 511
- Kormendy J., Kennicutt Jr. R. C., 2004, *ARA&A*, **42**, 603
- Kotilainen J. K., Falomo R., Scarpa R., 1998a, *A&A*, **332**, 503
- Kotilainen J. K., Falomo R., Scarpa R., 1998b, *A&A*, **336**, 479
- Kotilainen J. K., León-Tavares J., Olguín-Iglesias A., Baes M., Anórve C., Chavushyan V., Carrasco L., 2016, *ApJ*, **832**, 157
- Landt H., et al., 2017, *MNRAS*, **464**, 2565
- Laor A., 2000, *ApJ*, **543**, L111
- Leahy J. P., Williams A. G., 1984, *MNRAS*, **210**, 929
- Ledlow M. J., Owen F. N., Keel W. C., 1998, *ApJ*, **495**, 227
- León Tavares J., et al., 2014, *ApJ*, **795**, 58
- Lister M. L., Homan D. C., 2005, *AJ*, **130**, 1389
- Lister M. L., et al., 2016, *AJ*, **152**, 12
- Liu F. K., Chen X., 2007, *ApJ*, **671**, 1272
- Magorrian J., et al., 1998, *AJ*, **115**, 2285
- Mao M. Y., et al., 2015, *MNRAS*, **446**, 4176
- Mapelli M., Mayer L., 2012, *MNRAS*, **420**, 1158
- Mathur S., 2000, *MNRAS*, **314**, L17
- Mathur S., Fields D., Peterson B. M., Grupe D., 2011, preprint, ([arXiv:1102.0537](https://arxiv.org/abs/1102.0537))
- McMullin J. P., Waters B., Schiebel D., Young W., Golap K., 2007, in Shaw R. A., Hill F., Bell D. J., eds, *Astronomical Society of the Pacific Conference Series Vol. 376*, *Astronomical Data Analysis Software and Systems XVI*. p. 127
- Merritt D., Ekers R. D., 2002, *Science*, **297**, 1310
- Murgia M., Parma P., de Ruiter H. R., Bondi M., Ekers R. D., Fanti R., Fomalont E. B., 2001, *A&A*, **380**, 102
- Ohta K., Aoki K., Kawaguchi T., Kiuchi G., 2007, *ApJS*, **169**, 1
- Olguín-Iglesias A., Kotilainen J. K., León Tavares J., Chavushyan V., Anórve C., 2017, *MNRAS*, **467**, 3712
- Olguín-Iglesias A., Kotilainen J., Chavushyan V., 2020, *MNRAS*, **492**, 1450
- Orban de Xivry G., Davies R., Schartmann M., Komossa S., Marconi A., Hicks E., Engel H., Tacconi L., 2011, *MNRAS*, **417**, 2721
- Paliya V. S., Sahayanathan S., Parker M. L., Fabian A. C., Stalin C. S., Anjum A., Pandey S. B., 2014, *ApJ*, **789**, 143
- Pan H.-W., Yuan W., Yao S., Komossa S., Jin C., 2018, *ApJ*, **866**, 69
- Peterson B. M., 2011, preprint, ([arXiv:1109.4181](https://arxiv.org/abs/1109.4181))
- Pringle J. E., 1996, *MNRAS*, **281**, 357
- Rakshit S., Stalin C. S., Hota A., Konar C., 2018, *ApJ*, **869**, 173
- Ramos Almeida C., et al., 2012, *MNRAS*, **419**, 687
- Richards J. L., Lister M. L., 2015, *ApJ*, **800**, L8
- Ryan C. J., De Robertis M. M., Virani S., Laor A., Dawson P. C., 2007, *ApJ*, **654**, 799
- Shepherd M. C., Pearson T. J., Taylor G. B., 1994, in *Bulletin of the American Astronomical Society*. pp 987–989
- Sikora M., Stawarz L., Lasota J.-P., 2007, *ApJ*, **658**, 815
- Singh V., Ishwara-Chandra C. H., Sievers J., Wadadekar Y., Hilton M., Beelen A., 2015, *MNRAS*, **454**, 1556
- Taniguchi Y., 1999, *ApJ*, **524**, 65
- Wajima K., Fujisawa K., Hayashida M., Isobe N., Ishida T., Yonekura Y., 2014, *ApJ*, **781**, 75
- Wang F., et al., 2016, *ApJ*, **824**, 149
- Woo J.-H., Yoon Y., Park S., Park D., Kim S. C., 2015, *ApJ*, **801**, 38
- Yao S., Yuan W., Komossa S., Grupe D., Fuhrmann L., Liu B., 2015, *AJ*, **150**, 23
- Zhou H., Wang T., Yuan W., Lu H., Dong X., Wang J., Lu Y., 2006, *ApJS*, **166**, 128
- Zhou H., et al., 2007, *ApJ*, **658**, L13